Energy Reports 8 (2022) 8690–8700

Contents lists available at ScienceDirect

Energy Reports

journal homepage: www.elsevier.com/locate/egyr

Research paper

Performance improvements for the all-copper redox flow battery: Membranes, electrodes, and electrolytes

Wouter Dirk Badenhorst [a], Kuldeep [a], Laura Sanz [b], Catia Arbizzani [c], Lasse Murtomäki [a,*]

[a] Department of Chemistry and Materials Science, School of Chemical Engineering, Aalto University, PO Box 16100, 00076 Aalto, Finland
[b] Nvision System & Technologies S.L, Avenida Barcelona (ed ig nova Tecnoespai), 105 - DESP 8, Igualada, 08700, Barcelona, Spain
[c] Alma Mater Studiorum - University of Bologna, Department of Chemistry "Giacomo Ciamician", Via F. Selmi 2, 40126 Bologna, Italy

ARTICLE INFO

Article history:
Received 8 April 2022
Received in revised form 23 May 2022
Accepted 24 June 2022
Available online xxxx

Keywords:
Redox flow batteries
Hybrid flow cell
Ion exchange membrane
Cyclic-voltammetry
Renewable energy storage

ABSTRACT

The ever-increasing demand for renewable energy storage has led to the development of many energy storage systems, such as redox flow batteries (RFBs), including vanadium, iron–chromium, and the copper redox flow battery (CuRFB). A multitude of materials and electrolytes have been investigated to improve the performance of the CuRFB using an in-house manufactured cell. Using carbon ink coatings for the negative electrode and modern ion exchange membranes (IEMs), this version of the CuRFB was improved to current efficiencies above 95% with high voltage efficiencies of up to 81%, thereby improving energy efficiency by nearly 9% over the previous state of the art at 20 mA cm^{-2}. Additionally, the operating time of the CuRFB was significantly extended over 210 h of operation (50 cycles), 32% of the capacity remaining, without maintenance. Finally, stability of the new system with modern IEMs was proven by operation for over 1200 h operation, with over 300 charge and discharge cycles performed.

1. Introduction

Intermittent renewable energy requires significant energy storage infrastructure before industrial and domestic sectors can move towards full utilization of renewable energy sources (Castillo and Gayme, 2014). This infrastructure should store energy efficiently and be suitable for peak shaving during high production periods. Many storage systems are being re-explored in recent years for this purpose, such as kinetic (Rufer, 2020), thermal (Alva et al., 2018), and chemical energy storage systems (Castillo and Gayme, 2014), demonstrating that the diversification of energy storage technologies for the full integration of renewable energy into existing power grids is required. This diversification is needed as most storage systems have geographical limitations or cannot cover the wide ranges of power and energy requirements to support different services for the grid (peak shaving, load leveling, island, etc.). Electrochemical energy storage systems present significant advantages such as high efficiency and ease of installation in any location, including urban areas. In particular, Redox Flow Batteries (RFBs) present superior capabilities to provide massive amounts of energy storage, in the range of MWh, with high flexibility in selecting power-to-energy ratios, given that energy and power are decoupled in these types of systems. Vanadium redox flow batteries (VRFBs) have shown excellent performance in combination with photovoltaic power plants in the last few years (Sánchez-Díez et al., 2021; AlShafi and Bicer, 2021).

Other redox flow battery (RFB) storage technologies, such as zinc–bromine (Wu et al., 2017), iron–chromium (ICRFBs) (Zeng et al., 2016), organic RFBs (Leung et al., 2017), and the aqueous-all copper redox flow battery have been studied (Sanz et al., 2014). These RFB systems are highly applicable for large-scale energy storage due to their high storage capacity and reduced cost compared to other commercial battery systems (lithium-ion and lead–acid batteries) (Castillo and Gayme, 2014). Typical expenses associated with the VRFB range from 350–800 \$ $kW\ h^{-1}$, compared to 150–500 \$ $kW\ h^{-1}$ and 500–1500 \$ $kW\ h^{-1}$ for lead–acid and Li-ion batteries, respectively (Castillo and Gayme, 2014). As well as lower typical costs, RFBs typically have operational lifetimes above 20 years, compared to a projection of 3–10 years for lead–acid batteries and 10–15 years for Li-ion battery installations (Castillo and Gayme, 2014; Gouveia et al., 2020). These RFBs typically employ highly soluble redox couples in either aqueous or organic solutions as the charge carrier. During the charging of RFBs, the electroactive species are forced into a charged state by applying external power. At the same time, the electrolyte is circulated through an appropriate redox flow cell (RFC), and during discharge, the redox reaction is reversed, now supplying energy. In these RFBs, ion exchange membranes (IEMs) or porous

* Corresponding author.
E-mail address: lasse.murtomaki@aalto.fi (L. Murtomäki).

https://doi.org/10.1016/j.egyr.2022.06.075

separators are employed to prevent cross-mixing between the electrolytes of two half-cells and thus, avoid self-discharge and capacity loss of the RFB (Cho et al., 2019).

In the case of VRFBs, a highly selective membrane is required to prevent capacity decay over time (Cho et al., 2019). Additionally, they need high stability to prevent rapid membrane degradation due to the oxidative vanadium species present in the electrolyte (Sukkar and Skyllas-Kazacos, 2004). Therefore, typically VRFB membranes consist of highly fluorinated polymers for stability; however, high costs are associated with these perfluorinated membranes (Lloyd et al., 2015). In contrast, the ICRFB, first introduced in 1973, uses lower selectivity membranes by employing mixed-species electrolytes, which reduces cross-contamination. However, they often suffer from relatively high-capacity decay due to side reactions from the elevated voltages at which these systems operate (Ruan et al., 2020). Despite this, the meager price of the electrolyte negates this high-capacity loss, and ICRFBs have had some success during pilot plant operations. Compared to these RFBs, the CuRFB battery employs less aggressive electrolytes and can thus use lower-cost hydrocarbon-based separators. Furthermore, due to the relatively low cell voltage (0.65 V) in the CuRFB battery, most of the side reactions occurring in the ICRFB and VRFB systems are readily avoided.

In the CuRFB system, the three oxidation states of copper, Cu(s), Cu^{+}, and Cu^{2+} form a stable and reversible battery system. Both positive and negative half-cell electrolytes consist of equimolar amounts of Cu^{+}, which oxidize to Cu^{2+} in the positive half-cell during charging. At the same time, reduction of Cu^{+} takes place at the negative electrode in the negative half-cell to Cu(s), Eq. (1), and Eq. (2), respectively. Typically, Cu^{+} is not a stable form of copper in aqueous solutions but can be stabilized by adding excess amounts of chlorides (Sanz et al., 2013). During the subsequent discharge cycle, the deposited copper oxidizes back to the stable Cu^{+} chlorocomplex in the negative half-cell, and Cu^{2+} is reduced back to Cu^{+} in the positive half-cell. The presence of excess chloride ions is critical throughout this process to form an intermediate CuCl phase before redissolution occurs as $[CuCl_2]^{-}$ (Zhao et al., 2013). At low chloride content, passivation of the negative electrode during stripping can occur, significantly reducing the performance of the CuRFB system (Lloyd et al., 2015).

$$\textbf{Negative Half-cell}: \quad Cu^{+} + e^{-} \overset{\text{Charge}}{\rightarrow} Cu^{0} \tag{1}$$

$$\textbf{Positive Half-cell}: \quad Cu^{+} \overset{\text{Charge}}{\rightarrow} Cu^{2+} + e^{-} \tag{2}$$

The CuRFB system typically operates at lower voltages compared to the VRFB; however, the high solubility of copper in aqueous media (>3 M), single element composition, ease of electrolyte preparation, and easy recycling offset the low open current–voltage (OCV) (Sanz et al., 2014). In addition to its electrochemical properties, using copper within an RFB system offers several other benefits. One such benefit compared to vanadium is that copper is not considered a critical resource and has many well-established supply lines to all continents. In addition, established copper electrowinning processes and infrastructure can be used for copper recycling upon dismantling the CuRFB system (Beukes and Badenhorst, 2009).

Previous work regarding the CuRFB technology has brought some concerns when using copper as the active species and microporous separators (Sanz et al., 2014; Lloyd et al., 2015). The usage of microporous separators does reduce the overall cost of the CuRFB system due to their low cost (2 € m^{-2}) (Lloyd et al., 2015). However, these implementations suffered some significant drawbacks, such as rapid self-discharge of the CuRFB system due to low membrane selectivity, leading to the comproportionation between Cu^{2+} from the positive half-cell and the Cu(s) in the negative half-cell as shown in Eq. (3):

$$\textbf{Comproportionation}: \quad Cu^{2+} + Cu \rightarrow 2Cu^{+} \tag{3}$$

This self-discharge behavior was investigated previously by Lloyd et al. and self-discharge rates of approximately 3 mA cm^{-2} were found, which can become of concern during long-term operation or at low current densities (Lloyd et al., 2015). In addition, microporous separators are well known for high water transfer rates, affecting electrolyte concentrations (Wei et al., 2012). Finally, as the CuRFB is a hybrid phase system, additional concerns exist regarding the delamination of copper growth from the negative-half cell, leading to a capacity loss over time and the risk of dendritic copper growths.

This paper investigates multiple electrode modifications to the negative half-cell to increase copper adhesion quality during operation using a 25 cm^2 in-house manufactured redox flow cell (RFC) to address these limitations and concerns. In addition to this, we will test a variety of different polymeric membranes obtained from Daramic, FuMATech GmbH, and SUEZ Water Technologies & Solutions. Finally, this paper will evaluate the usage of these membranes for the CuRFB system for over 50 deep cycles to ascertain long-term membrane stability and capacity retention of the CuRFB, with over 300 charge and discharge cycles using the FAP-330 membrane.

2. Experimental

2.1. Copper electrolyte

Various Cu(I) electrolytes were prepared using the comproportionation reaction shown in Eq. (3). First, the required amount of 6 M HCl solution using 37% HCl (ACS reagent, Sigma Aldrich) and deionized water was prepared, then the solution was purged with N_2 for 30 min to remove dissolved oxygen. To this solution, equimolar amounts of Cu(II)Cl (97% purity, Sigma Aldrich) and Cu(s) powder (<425 μm, >99.5% purity, Sigma Aldrich) were added to prepare the 0% state of charge (SOC) electrolyte. In some cases, 2 M of $CaCl_2 \cdot H_2O$ (granular $\leq$ 7.0 mm, $\geq$ 93.0% purity, Sigma Aldrich) was added to the electrolyte to increase the copper to chloride ratio. Finally, to facilitate the comproportionation reaction, the electrolyte was kept under an N_2 atmosphere and stirred at elevated temperatures (40 °C). Complete comproportionation is indicated by a transition of the electrolyte color from dark brown to a colorless state. Due to the chloride complexes, a mixture of Cu^{+} and Cu^{2+} exhibits a dark brown color with even minor Cu^{2+} present, whereas a solution of Cu^{+} is colorless (Lloyd et al., 2015).

2.2. Cyclic voltammetry

Cyclic voltammograms (CVs) were obtained using a typical three-electrode electrochemical cell (Autolab PGSTAT12), with glassy carbon (5 mm diameter, HTW Hochtemperatur-Werkstoffe GmbH) as the working electrode, a copper rod (99.99+ % purity, Sigma Aldrich) as the counter electrode, and using a standard Ag/AgCl reference electrode. The CVs were conducted at a scan rate of 100 mV/s, between −0.75 V and 1.0 V (vs Ag/AgCl), while an inert atmosphere (N_2) was kept to prevent oxygen ingress into the solutions. Additionally, the electrolyte was heated to 60 °C using a circulating thermostatic water bath. In addition to the GC working electrode, modified electrodes were tested, where a GC tip coated using either the Peters SD 2843 HAL or the Creative Materials 119–28 carbon ink was used. Then, the carbon inks were applied to the GC electrode with a layer thickness of 0.2 mm. Finally, the carbon ink was post-processed as indicated by the manufacturer's specifications.

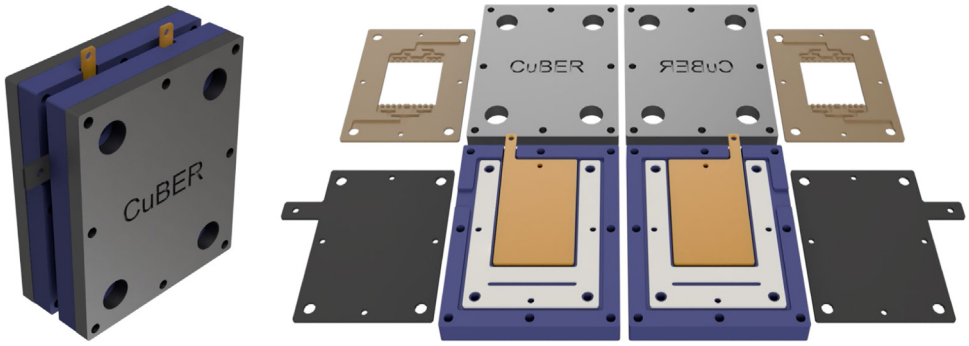

Fig. 1. Renders of the redox flow cell used in this study to determine the effects of various parameters on the performance of the CuRFB battery system.

2.3. Redox flow cell

A traditional (sandwich type) redox flow cell (RFC) was designed for testing with an active electrode and membrane area of 25 cm^2 (5 ×5 cm) and an anode–cathode distance (ACD) of 4 mm, of which the design is shown in Fig. 1. For the positive half-cell, an SGL carbon FR-10 bipolar plate was employed together with a Cera Materials PAN carbon felt with a thickness of 1/8" (37% compression); thermal treatment of the PAN felt was performed as described previously (Faggiano et al., 2022). The same SGL FR-10 bipolar plate was used for the negative half-cell, in either pristine condition or with an added 0.2 mm thick layer of carbon ink (CM 119-28) applied and post-processed to the manufacturer's specifications. Additionally, reverse osmosis spacers were employed for the negative half-cell with a thickness of 2 mm with 4.3 × 4.3 mm openings to prevent excessive membrane flexing. Silicone gaskets were used where required to seal the unit entirely, with the endplates being manufactured from PVC-U, the compression plates from aluminum, and the system was torqued to 4 N m. For both the negative and positive half-cell, the bipolar plate was in contact with a copper current collector to minimize contact losses, to which the electrical leads were connected. Using a Keithley 2420 source measure unit (SMU), the IR drop between the power source and the copper current collectors was determined and compensated.

Thermal management of the system was achieved through immersion of the electrolytes in a HAAKE B3 water bath, and heating for the RFC was achieved with two 10-watt silicone heating pads (RS-Components) together with a Raspberry Pi Pico using MCP9601 thermocouple sensors (K-type). The system was operated at 60 °C to improve charge and discharge performance by adding thermal energy according to the Nernst equation, improving electrode reaction kinetics, and improving the solution conductivity (Lacarbonara et al., 2021). Circulation of both the negative and positive half-cell was achieved using an Ismatec peristaltic pump, using 2-stop tubing with appropriate inner diameters to achieve a flow rate of 30 mL min^{-1} for each half-cell (0.5 cm s^{-1} superficial flow velocity). The electrolytes were housed in sealed glass containers, and a slight N_2 overpressure was maintained in the system to prevent oxygen ingress as best possible. The standard experimental conditions used during the operation of the RFC are listed in Table 1; all tests were conducted from 0% SOC up to the maximum achievable SOC, which correlates to the voltage cut-offs of 0.3 V for discharge and 0.9 V for charging, respectively. Charging and discharging was achieved using either a Keithley 2420 source meter unit, controlled through an RS-232 connection and custom control software written in Rust, or using a Lahne G340 A battery testing system and its included software.

At the standard conditions listed above, the theoretical capacity amounts to 53.6 Ah L^{-1}, and for the 50 mL solution, 2.68 Ah. For the testing, four different membranes were tested with their manufacturers' specified parameters being listed below (see Table 2):

Table 1
Standard experimental conditions employed during the redox flow cell operation, unless stated otherwise.

Parameter	Value	Parameter	Value
HCl (M)	6	Electrolyte Volume (mL)	50
CuCl (M)	2	Flow Rate (mL min^{-1})	30
Temperature (°C)	60	Current density (mA cm^{-2})	20
Low Cut-off (V)	0.3	Bipolar Plate	SGL FR-10
High Cut-off (V)	0.9	Carbon Felt Sheet	PAN
Number of Cycles	3	Carbon Ink Coating	CM 119-28

2.4. Cycling stability

The long-term cycling stability of the FAP-330 and the AR-118 membranes were tested using retrofitted PermeGear® permeation cells. Using a water circulation heating pump (Thermo Scientific™ SC150), the electrolytes were kept at 60 ± 1 °C with charging and discharging achieved by the Lahne G340 A battery cycler. Each compartment was filled with 3 mL of electrolyte and stirred using magnetic stirring bars. A graphite rod was employed for the positive electrode (diameter: 3.25 mm, length: 25 mm), with the negative electrode consisting of a wound platinum wire (diameter: 1 mm, length of coil: 15 mm). Both electrodes employed had a surface area > 1 cm^2 with 20 mA being applied during both charging and discharging for a resultant 20 mA cm^{-2} with regard to the membrane surface area. Additionally, this experimental configuration was employed to determine the self-discharge rates of the ion exchange membranes and extended testing for the FAP-330 (over 300 charge–discharge cycles).

3. Results and discussion

3.1. Negative electrode

With the CuRFB being a hybrid system, as one electroactive species deposition occurs, stable growth is essential for stable long-term operation (Fraser et al., 2020). Unstable copper deposition or uneven copper stripping can lead to an eventual loss of capacity and a decrease in current efficiency since the amount of copper available during discharge is reduced (Sanz et al., 2014). Fig. 3 shows the CVs obtained of the three different working electrode materials in the electrolyte of 2 M CuCl and 6 M HCl at 60 °C with the scan from 0 V to negative potentials. The copper nucleation reaction starts at approximately −0.3 V irrespective of working electrode material, with reduction peaks observed at −0.5 V for the SD 2843 HAL and CM 119–28 working electrodes.

Table 2
Membrane properties taken directly from suppliers' specification sheets.

Membrane	Thickness (μm)	Porosity (%)	Specific resistance (mOhm cm^{-2})	Ion exchange capacity (meq g^{-1})
Daramic-CL	350	58	<220	–
FAP-330	30	–	<400	1.20
FS-990	95	–	<300	1.18
AR-118	130	–	<1100	2.35

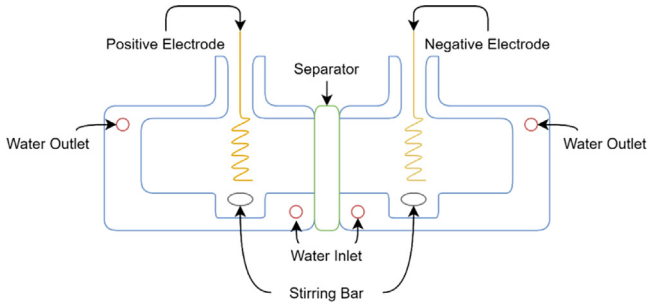

Fig. 2. Schematic illustration of retrofitted PermeGear® permeation cell used for cycling stability and self-discharge rate determination.

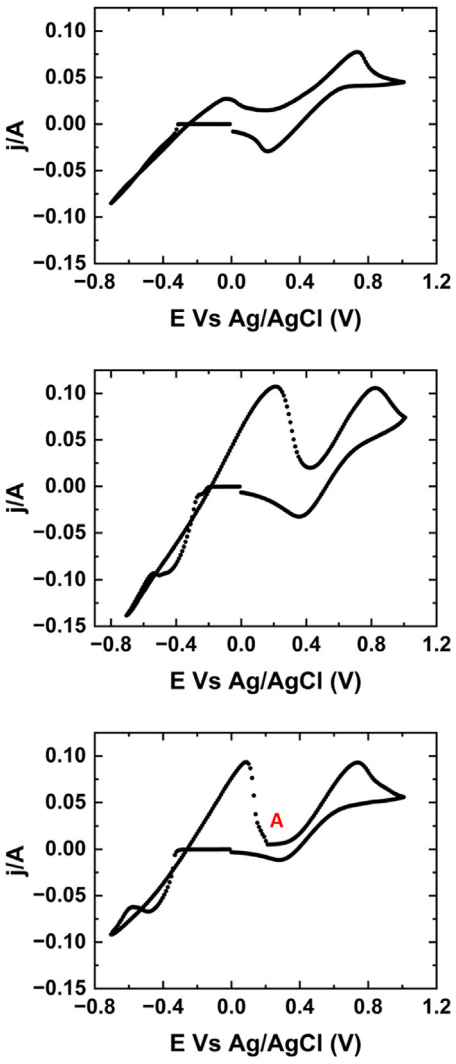

Fig. 3. Cyclic voltammograms with three different working electrode surfaces; Glassy carbon (A), SD 2843 HAL (B), and CM 119–28 (C), in a solution of 2 M CuCl and 6 M HCl at 60 °C with a scan rate of 100 mV s^{-1}.

For both the SD 2843 Hal and CM 119–28 explicit nucleation loops appear, indicating that the amount of available nucleation sites increases over time.

In contrast, in the case of the clean, glassy carbon electrode, no maximum reduction peak is observed, with current linearly increasing as the voltage decreases. For the bare GC electrode, the current efficiency for the deposition and stripping is 39% compared to 97% and 96% obtained for the SD 2843 HAL and CM 119–28 GC coated electrode, respectively. While previous work (Sanz et al., 2014) has obtained higher current efficiencies of 85% on bare GC, these scans were performed to −0.2 V vs (Cu/Cu^{+}). Comparatively, in this paper, the scans were performed to more negative potentials where side reactions are more likely (hydrogen evolution). In addition to this, during testing of the bare GC working electrode, copper particles were visible at the bottom of the three-electrode flask, indicating that a significant fraction of the copper was delaminated from the GC surface, further demonstrating the need for electrode modifications to achieve stable copper deposition.

The carbon ink coatings seem to affect the redissolution behavior of the deposited copper to Cu^{+}, showing significantly higher reduction currents and oxidation peak values. Some of this higher current value can be ascribed to a slight increase in surface area due to the applied coating. The irregular carbon ink surface is shown in Fig. 1A in the supplementary materials. However, it is more likely that the coating is causing uneven copper growth, leading to an increase in the availability of nucleation sites over time, as indicated by the nucleation loop being present for both coating materials (Bard and Faulkner, 2001; Nieminen and Murtomäki, 2021). When observing the copper redissolution for the CM 119–28 coating, a dramatic drop in current indicates fast redissolution of the copper. Additionally, a slight deflection in the discharge current behavior (marked A) is ascribed to two-step copper redissolution, as reported by several other researchers (Starosvetsky et al., 2006; Kologo et al., 2007). The copper redissolution from the CM 119–28 coating is not severely slowed down by the formation of the CuCl intermediary step, as at higher scan speeds (up to 500 mV s^{-1}, not shown), no peak broadening was observed (Starosvetsky et al., 2006).

Using the Daramic-CL separator and the RFC at a current density of 25 mA cm^{-2}, multiple charge and discharge cycles were performed using each of the electrode materials. In the case of the SD 2843 HAL coating, the ink could not adhere firmly to the bipolar plate, and the carbon ink and the copper deposit delaminated during the first cycle. With no electrode modifications, voltage efficiency (VE, obtained by using the average charge and discharge voltage) and current efficiency (CE, obtained by integration of charge and discharge current) values of 41% and 53%, respectively, were obtained compared to the 75% and 62% with the CM 119–28 coating. The improvement of the voltage efficiency is attributed to the increase of available nucleation sites over time, as seen with the CVs, with the subsequent increase in electrode surface area leading to lower overpotentials.

This idea of increased electrode area is supported by scanning electron microscopy (SEM) images of the copper growth on the CM 119–28 coating (Fig. 4), showing highly amorphous phases. Unfortunately, SEM images for the copper growth on the clean bipolar plate could not be produced as the copper separates

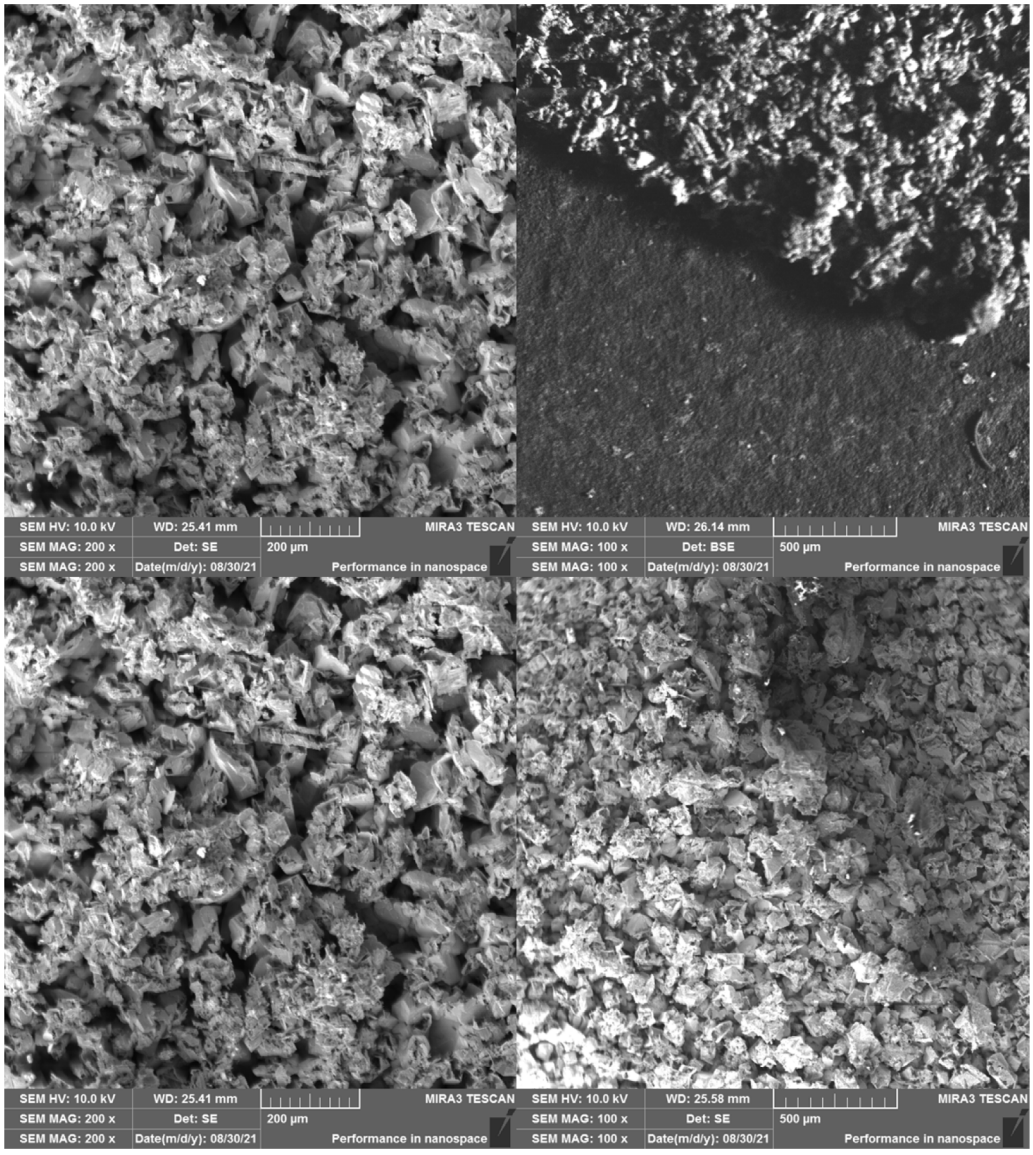

Fig. 4. Scanning electron microscopy images of copper growth on the CM 119–28 coating at 25 mA cm^{-2} and 60 °C using the Daramic-CL separator at a magnification of ×100 (left) and ×500 (right) .

from the bipolar plate during disassembly (Fig. 2A, supplementary materials). This increased surface area, together with the fast redissolution observed during the CV study, shows that the CM 119–28 is a highly functional coating for copper deposition in the CuRFB. In addition, the higher CE observed indicates that the copper growth on the CM 119–28 attaches more strongly than the clean bipolar plate. A reduced amount of copper powder was observed in the system when using the CM 119–28 coating compared to operation with the pristine bipolar plate. Without this coating a large amount of delaminated copper visible in the flow divider (Fig. 2A) supplementary materials).

In previous attempts to improve the performance of the negative electrode in the CuRFB system, Leung et al. (2017) explored the use of metallic electrodes (titanium and stainless steel). While these provided improvements in current efficiency due to the increase in metal–metal adhesion and small grain size copper formation resulting in improved mechanical properties, no significant improvements in voltage efficiency were obtained. Comparatively, the growth observed on the CM 119–28 coating does not have a well-defined grain structure, which provides a larger surface area for the reactions and reduces overpotentials. Thus, the voltage efficiency is improved. Looking at the copper structure in Fig. 2A (supplementary materials), the pristine bipolar plates formed solid copper structures, compared to high area copper structures when using the CM 119–28 coating.

Additionally, the copper growth on the CM 119–28 coating shows reduced voids in the copper growth compared to the copper growth structures observed on the titanium and stainless steel electrodes in previous works (Sanz et al., 2014). Therefore, it is obvious that the copper morphology directly affects both deposition and redissolution processes, which dramatically impacts the performance. In this regard, CM 119–28 is a promising alternative negative electrode for the operation of a high-performance CuRFB system, additionally offering improved stability compared to metallic electrodes, which would slowly deteriorate in a highly acidic media (Martinez-Lombardia et al., 2014).

3.2. Membrane selection

In previous iterations of the CuRFB system, low-cost porous separators, such as the Daramic-CL and Amersil-sil S10, were used (Lloyd et al., 2015). Usually, hydraulic pressure differences

Table 3
Average voltage and current efficiency of three cycles using the redox flow cell with four different membrane separators.

Membrane	VE (%)	CE (%)	EE (%)
Daramic-CL	79	59	47
FS-990	70	83	58
FAP-330	81	90	73
AR-118	69	87	60

Table 4
Rates of self-discharge for various membranes tested in the CuRFB system.

Membrane	CE_{avg} (%)	SD (mA cm^{-2})
Daramic-CL	64.58 ± 2.37	N/A
FAP-330	98.21 ± 0.13	0.64 ± 0.15
AR-118	93.29 ± 0.11	3.39 ± 0.38

may cause high water and electroactive species transfer through the membrane when using porous membranes, which degrades performance and cause a charge imbalance over time in the RFB (Wei et al., 2012). This low selectivity causes a high self-discharge rate in the CuRFB battery, with values of 3 mA cm^{-2} reported for Daramic-CL previously at 50% SOC. Therefore, Lloyd et al. (2015) operated the CuRFB at current densities above 50 mA cm^{-2} to achieve current efficiency values above 90%. However, operation at these high current densities leads to reduced energy efficiency (EE) values due to excessive overpotentials at both the positive and negative half-cells.

Three IEMs were evaluated for their usage in the CuRFB system as an alternative to the porous Daramic-CL. These IEMs should allow for the operation of the CuRFB system at lower current densities and higher CE values, resulting in more useable DC–DC efficiencies. Table 3 shows the average VE, CE, EE values for the four membranes tested at the standard conditions within the RFC. Both FS-990 cation exchange membrane (CEM) and AR-118 anion exchange membrane (AEM) show lower voltage efficiency compared to the Daramic-CL. The low voltage efficiency of these two membranes is attributed to their low conductivity and high thickness of 85–105 μm and 110–130 μm. Conversely, the AEM FAP-330 membrane has a higher conductivity and a lower thickness of 27–33 μm and provides similar conductivity to Daramic-CL. In addition, due to reduced copper transport by IEMs, the CE of the CuRFB process is greatly improved from 59% to more than 85% compared to Daramic-CL, which is attributed to reduced Cu(II) crossover to the catholyte, leading to a reduced amount of Cu(II) comproportionating with the formed Cu(s) on the negative electrode. Therefore, the use of the FAP-330 membrane results in a substantially higher average EE of 73% compared to previously reported values of 45% and 68% using Amersil-sil S10 (porous separator) and Daramic-CL, respectively (Sanz et al., 2014; Lloyd et al., 2015).

Fig. 5 shows the charge and discharge curves for Daramic-CL, FS-990, FAP-330, and AR-118 membranes, where distinct behaviors can be noted. For all membranes except AR-118, the charging time is approximately 5 h, compared to the theoretical charging time of 5.3 h for 100% SOC at 20 mA cm^{-2}. Indicating that due to the high specific resistance of this membrane (<1100 mΩ cm^{-2}), the system cannot reach high SOC levels before the cut-off voltage of 0.9 V is reached, which is further corroborated by results shown in Section 3.4. Regarding the performance of Daramic-CL, while initially high SOC levels are achieved, it can be noted that the discharge time decreases by nearly 30 min after each cycle, indicating a fast capacity decay rate. The fast capacity decay when using Daramic-CL is attributed to Cu(II) and Cu(I) transfer to the catholyte where the Cu(II) comproportionates with the Cu(s). This followed by the subsequent lack of Cu(II)/Cu(I) at the positive electrode limiting charge and discharge, also verified by the color change in the catholyte from clear Cu(I) electrolyte to a mixture of Cu(II)/Cu(I) which is dark brown. In addition to this capacity decay, the voltage performance of Daramic-CL performed significantly worse compared to FAP-330, which indicates despite the low specific resistance of 220 mΩ cm^{-2}, the membrane has a high ohmic resistance leading to low voltage efficiency. This behavior of porous separators is expected as their conductivity typically is due to the electrolyte filling the pores, not the membrane properties. Finally, with FS-990 as the CEM, relatively little drift in the discharge time is seen, indicating a low crossover rate of Cu(II)/Cu(I) from the anolyte to the catholyte and preferential transport of protons over the copper species. Unfortunately, the high ohmic resistance observed during testing severely hampered the performance metrics via a low voltage efficiency.

Using retrofitted PermeGear cells, the self-discharge rate, without losses caused by the deposition and stripping process, was determined. Firstly, the system was charged to 100% SOC and subsequently discharged back to 0% SOC repeatedly to obtain an average current efficiency (CE_{avg}) which includes deposition, stripping, and self-discharge losses. This was followed by charging the system to 100% SOC, after which zero current was applied to the system, and the open current–voltage (OCV) was measured for 5 h, after which the system was discharged back to 0% SOC. The self-discharge rate was then determined where Q_C is the charge capacity in mAh, Q_D is the discharge capacity in mAh, A is the membrane area in cm^2, and t_{rest} is the OCV measurement time in hours using Eq. (4).

$$\mathrm{SD}\left(\mathrm{mA\ cm^{-2}}\right) = \frac{(CE_{\mathrm{avg}} \cdot Q_C - Q_D)}{A \cdot t_{rest}} \tag{4}$$

These results indicate that FAP-330 shows increased selectivity towards anionic species over the Cu^+ and Cu^{2+} species, with a self-discharge rate of 0.64 ± 0.15 mA cm^{-2} (Table 4). This self-discharge rate is several times smaller than the previously reported value of 3 mA cm^{-2}, obtained at 50% SOC, for Daramic-CL and is consistent with the high CE noted for the FAP-330 earlier (Lloyd et al., 2015). Equally, AR 118 V showed a higher self-discharge rate of 3.39 mA cm^{-2}, which is in line with the observed OCV drop over the resting period. These values indicate a substantial improvement over the previously reported values for Daramic-CL, as the previous values were obtained at 50 % SOC which has a significantly lower osmotic pressure driving the movement of the copper species compared to testing at 100% SOC. The self-discharge rate of FS-990 was not determined, as it is not suitable for implementation with the high overpotentials noted in Fig. 5.

During the 5-hour resting period (Fig. 6), the OCV for FAP-330 decreased by 5.9 ± 0.4 mV, whereas it decreased by 21.0 ± 1.2 mV for the AR 118 V, which correlates with the calculated self-discharge values (Table 4). Daramic-CL showed a near 60.5 mV drop over the first resting period and a 74.1 mV drop over the second rest time (data is not shown). The electrolyte color shows a deep dark brown color for the catholyte, indicating a high presence of Cu(II) in the catholyte and suggesting that a large amount of Cu(II) transfer has occurred. This charge imbalance then causes the dissolution of any plated Cu(s) on the negative electrode leading to a loss of SOC and a subsequent decrease in capacity. The self-discharge rate is highly dependent on the concentration of Cu^+ and Cu^{2+} species in the positive half-cell compared to the Cu^+ concentration in the negative half-cell. To get a more accurate understanding of the self-discharge rate of these membranes in the CuRFB system, an analysis of this effect at various SOC levels would be required. An ongoing investigation is looking into UV–Vis spectroscopy to provide insight into

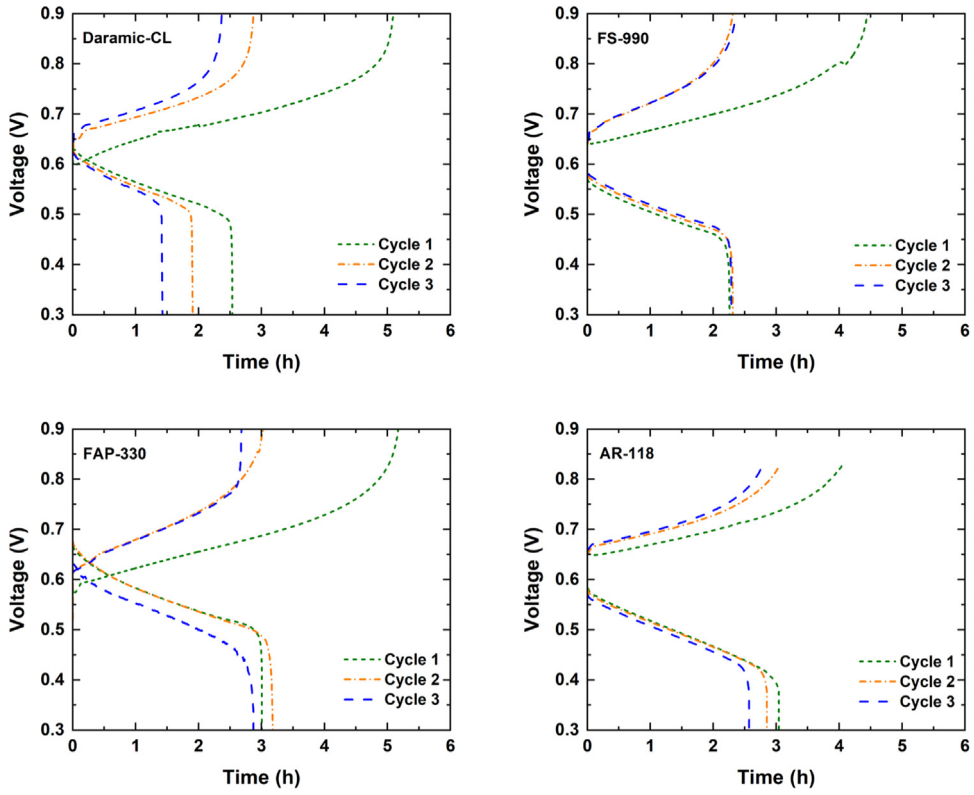

Fig. 5. Charge and discharge curves for each of the four membranes tested with 2 M Cu(I)Cl, 6 M HCl at 60 °C with a current density of 20 mA cm^{-2}.

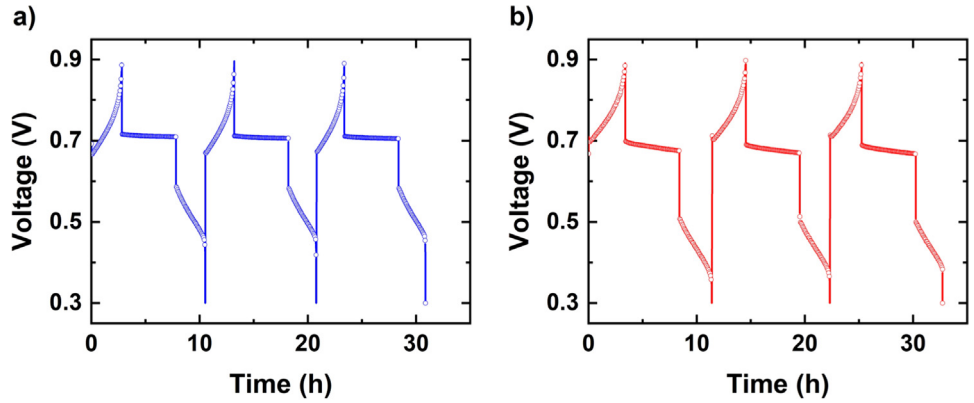

Fig. 6. Self-discharge curves of the FAP-330 (a) and AR-118 (b) membrane with a rest time of 5 h after being charged to the maximum state of charge.

which copper species are preferentially transported through the membrane, if any.

3.3. Copper utilization

Work conducted by Lloyd et al. found that during initial cycles, approximately 70–80% of the copper in the electrolyte is utilized; however, the electrolyte utilization rapidly drops to only 55% after the third cycle and continues to decrease due to copper delamination and self-discharge mechanisms (Lloyd et al., 2015). To address the copper utilization, a variety of copper solutions with different copper to chloride ratios were investigated, as previous work has shown that copper kinetics are dependent on chloride content and temperature (Sanz et al., 2013). For fast reaction kinetics, it has been suggested that a Cu:Cl ratio greater than 1:5 should be used in the CuRFB when operating at temperatures of 60 °C (Sanz et al., 2013). Work by Lacarbonara et al. indicated that a ratio of 1:5 provided the best performance (Wei et al., 2012). Similarly, as the redissolution of Cu(s) goes through the intermediary of CuCl before the formation of the soluble $CuCl_2^-$, a low Cu:Cl ratio can reduce the reaction rate and passivate the electrode. Therefore, to increase the copper utilization, varying Cu:Cl ratios were examined using FAP-330 due to its excellent performance thus far in the RFC, Table 5. In cases where only 1 M Cu(I)Cl was used in the electrolyte, the volume was increased to 100 mL to keep the total copper content unchanged and to keep the capacities directly comparable with a theoretical capacity of 2.68 Ah.

Table 6 reports voltage efficiency, current efficiency, and both charge and discharge capacities for FAP-330 with the electrolytes listed in Table 5 for 3 subsequent cycles each. The first thing to note would be that electrolytes 206 and 106 reached 97% and 98% of maximum SOC compared to electrolytes 226 and 126, only reaching 55% and 51% of maximum SOC. This maximum SOC behavior strongly indicates that the conductivity loss experienced

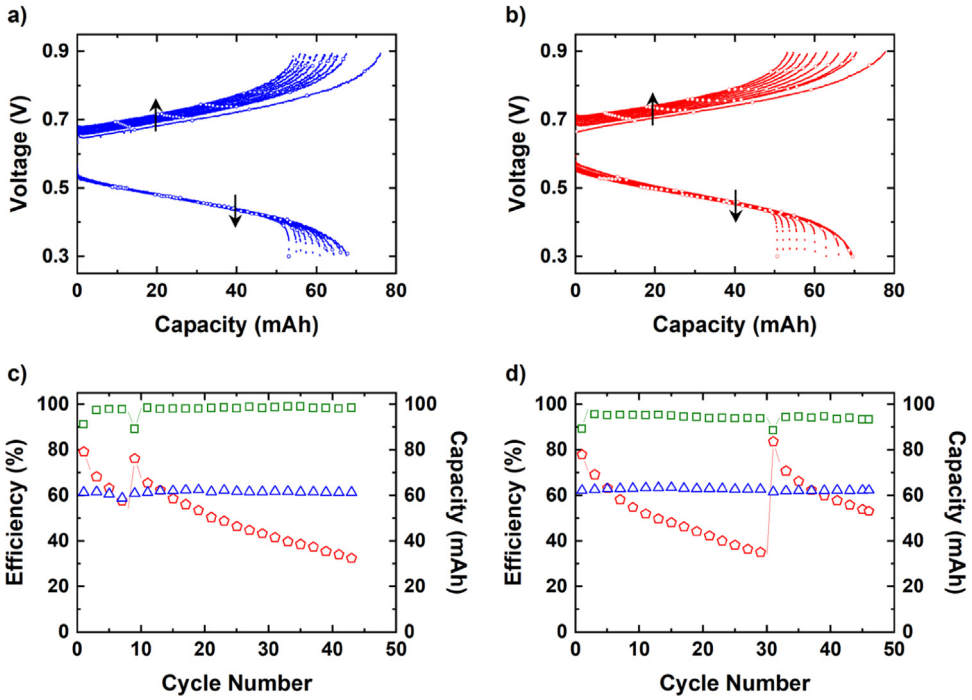

Fig. 7. Voltage capacity and performance for the first 50 cycles of the retrofitted PermeGear for both the FAP-330 (a, c) and the AR-118 (b, d) membranes.

Table 5
Electrolyte configurations tested in the redox flow cell to determine copper to chloride ratio effects on copper utilization during operation of the copper redox flow battery.

Electrolyte #	CuCl (M)	$CaCl_2$ (M)	HCl (M)	Cu:Cl
206	2	0	6	1:4
226	2	2	6	1:6
106	1	0	6	1:7
126	1	2	6	1:11

Table 6
Table showing the voltage efficiency (VE), current efficiency (CE), charge capacity (Q_C), and discharge capacity (Q_D) for the FAP-330 membrane employing differing electrolyte compositions.

Electrolyte	Cycle	VE (%)	CE (%)	Q_C (Ah)	Q_D (Ah)
206	1	83	58	2.59	1.50
	2	81	96	1.58	1.52
	3	80	92	1.46	1.34
226	1	76	85	1.48	1.26
	2	76	86	1.25	1.10
	3	81	45	1.08	0.49
106	1	78	73	2.65	1.92
	2	69	93	1.47	1.37
	3	68	92	1.32	1.22
126	1	76	88	1.36	1.19
	2	76	91	1.16	1.05
	3	78	84	1.02	0.86

after adding the $CaCl_2$ overshadows the potential benefits from increasing the chloride to copper ratio. And is supported by work done by Lacarbonara et al. showing that the addition of 1 M $CaCl_2$ to 2 M Cu, 6 M HCl reduces the conductivity from 812 mS cm^{-1} to 634 mS cm^{-1} at 40 °C. Consequently, the solutions containing $CaCl_2$, despite having a higher chloride to copper ratio, lower SOC values are reached before the 0.9 V cut-off voltage. Additionally, $CaCl_2$ as an additive seemingly reduces the current efficiency, which is attributable to a less optimal copper growth pattern; it is well known that additives have a significant effect on the copper growth pattern (Wei et al., 2012).

Alternatively to adding $CaCl_2$ to increase the chloride to copper ratio, the concentration of the copper can be decreased while keeping the HCl concentration at 6 M. When looking at electrolyte 106 compared to electrolyte 206, a 9% drop in voltage efficiency is observed. However, the first cycle current efficiency is greatly improved, from 58% with electrolyte 206 up to 73% with electrolyte 106. This reinforces findings in the literature that increasing the chloride to copper ratio increases the discharge kinetics by preventing negative electrode passivation (Sanz et al., 2014, 2013). While this does not present a clear best-performing electrolyte composition as the 15% improvement in useable copper comes at the cost of a 9% voltage efficiency decrease, this provides a clear heading for future electrolyte work.

3.4. Cycling stability

Both FAP-330 and AR-118 membranes were tested in the miniaturized RFC for nearly 50 cycles (0% to maximum% SOC), with earlier work reaching a similar 43 cycles using porous Daramic separators. The voltage response to the decrease in capacity is shown in Fig. 7.a and Fig. 7.b for the first 10 cycles. In addition, the VE, CE, and capacity is also shown over the first 50 cycles in Fig. 7.c and Fig. 7.d. It can be seen from Fig. 7.b, AR-118, that there is a considerable capacity loss per cycle, and the discharge voltage is slightly affected by the capacity decay. Comparatively, Fig. 7.a, FAP-330, shows reduced capacity decay, and the discharge voltage seems to be independent of this phenomenon. However, in both cases, the charging voltage shows a strong upward trend over time and is attributed to undischarged Cu^{2+} and decreasing Cu^{+} concentrations. As less Cu^{+} is available at the positive electrode, mass transfer effects become relevant, raising the overpotential (due to diffusion and charge transfer).

Capacity loss rate was determined for both membranes, where FAP-330 showed a capacity loss rate of 1.06 mA cm^{-2} over the 50 cycles and AR-118 showed a slightly higher rate of 1.49 mA cm^{-2}. These results indicate that AR-118 shows lower selectivity compared to FAP-330 towards anionic species over the Cu^{+1} and Cu^{+2} species. The self-discharge rates determined for the

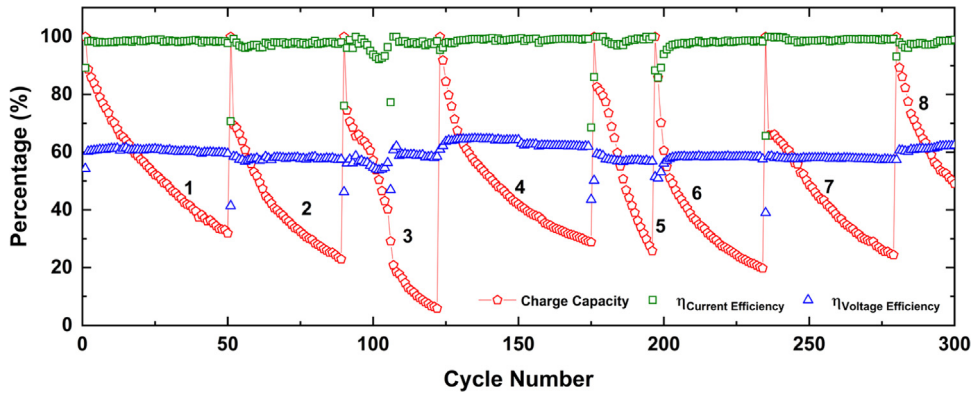

Fig. 8. Testing of the FAP-330 membrane for 300 cycles (1200 h, 50 days) using the retrofitted PermeGear cell, with the electrolytes being changed whenever the capacity dropped below 20% of the initial capacity.

two CuRFB configurations from the 50 cycles of operation are in line with the determined values from earlier self-discharge estimations. However, the 50 cycles of operation add additional information that the self-discharge rate is not linear, with the capacity loss slope changing over time. This behavior is expected because when the concentration difference between the two half-cells decreases over time, the osmotic driving force is reduced, slowing the self-discharge rate.

Approximately 55% of the capacity was decayed from cycle 10 to cycle 44 (170 h) using the FAP-330 membrane. Compared to previous work, a rapid decay in capacity (55%) was observed in only 9 h, when the CuRFB was operated with the Daramic-CL at a current density of 50 mA cm^{-2} (Lloyd et al., 2015). Therefore, despite the higher cost of these separators compared to the low-cost Daramic-CL alternatives, their performance improvements are significant and ease the operation of the CuRFB system substantially. Furthermore, the FAP-330 showed excellent stability, achieving CE values of >98.5%. This value only dropped during the first cycle (Fig. 7.a) and after the electrolyte regeneration (discussed later), but remained consistent over the testing period. Comparatively, the AR-118 membrane shows slight degradation in performance, showing initial CE values of 95.2% before dropping to 93.4% at cycle number 46.

For additional insight into the stability of the membranes in the CuRFB electrolyte, SEM images of membranes were obtained after they had been used for cycling for well over 200 h and are available in the Supplementary Materials. No actual deterioration of the membrane surface is visible after the use for over 200 h.

In this paper, we have shown that it is possible to exploit the single active redox element nature of the CuRFB in addition to copper comproportionation effects (Eq. (3)) to restore decayed capacity. Capacity regeneration was achieved by mixing both the anolyte and catholyte, allowing excess Cu(II), caused by charge imbalance to react with delaminated copper or unused copper in the negative half-cell. In the case of the FAP-330 configuration, the capacity decayed from 79 mA h initially to 54 mA h after cycle 8; after regeneration, the capacity was increased again to a value of 76 mA h, that is 96% of the initial capacity (Fig. 7.c).

Finally, to determine the stability of the proposed CuRFB system, 300 charge and discharge cycles were conducted using the FAP-330 membrane and electrolyte 106. The charge capacity was normalized to the maximum value achieved in the first cycle after electrolyte refresh. Over 300 cycles, average current efficiencies of 97% and energy efficiency of 59% were achieved. On average, the CuRFB operated over 150 h before charge capacity dropped to between 30% and 20%, after which the electrolyte was refreshed. This average was lowered by runs 3 and 5 in Fig. 8 where copper delamination occurred, leading to a sharp drop in charge capacity. The first run was charged and discharged 50 times within 210 h, with the capacity dropping to 32% at the end. Over 300 cycles, no significant decrease in current efficiency was observed. The capacity loss behavior remained relatively consistent, indicating that the proposed system is more stable and useable than previous work.

In Table 7, the performance parameters of previous CuRFB work are tabulated together with results from this work. The same cut-off voltage and temperature were used in both papers, with the differences stemming from the component and electrolyte choices investigated in this paper. The critical improvement comes from the increase in the current efficiency from approximately 73% to over 96%, which is attributed to the lower self-discharge rate when using the modern IEMs compared to the porous separator employed previously. This is further exemplified by the previous work showing that when the CuRFB was operated with the older material choices at 50 mA $cm^{-2,}$ the capacity faded to 58% after the initial cycle, followed by the capacity decreasing to 3% the theoretical capacity within 9 h (Lloyd et al., 2015). Whereas compared to run 1, using electrolyte 106, in Fig. 8, the run charged up to 95% of the theoretical maximum, dropping to 85% of the theoretical value after the first cycle and then declining to 32% of the maximum first charge over the timespan of 210 h. Therefore with the new materials and electrolytes, a capacity loss rate of 0.3% per hour of the maximum occurs, compared to 6% per hour when employing the Daramic-CL separator for a 20 times lower capacity loss rate.

4. Conclusions

In this work, various steps to understand the CuRFB battery's operation on a macro level have been taken, opening the way for future research into specific aspects affecting the performance of the CuRFB system. Adhesion and copper morphology has been improved on bipolar plates typically used in RFBs, using carbon ink coatings, compared to the pristine bipolar plates and metallic electrodes used previously. The CV showed explicit nucleation loops when using these inks — leading to improved current efficiencies from 41% to 75% and the voltage efficiency from 53% up to 62%, using the Daramic-CL separator. Further improvements to the CuRFB were made by electrolyte variation, leading to a change in the chloride to copper ratio by reducing copper content to 1 M while using 6 M HCl, leading to a higher first cycle utilization and continued capacity utilization of approximately 73%.

In addition to these improvements, both the stability and performance of the CuRFB was enhanced through the use of the FAP-330 separator, offering low self-discharge rates of 0.64 mA cm^{-2} at 100% SOC. Additionally, high separator stability using the FAP-330 was observed after operation for over 1200 h resulted in an

Table 7
Performance comparison between this work and work done by David Lloyd et. al. (Cho et al., 2019) on the CuRFB system.

Parameter	Lloyd et. al[a] 20 mA cm^{-2}	This work[a],[A] 20 mA cm^{-2}
CE (%)	≈73	95
VE (%)	≈94	81
EE (%)	≈68	77
SD (mA cm^{-2})	3	1
Parameter	**Lloyd et al.** [b] **50 mA cm^{-2}**	**This work[B] 20 mA cm^{-2}**
Maximum operating time (h)	9	210
Remaining capacity at end (% of initial)	3	32

[a]Electrodes: (Graphite foil), Electrolyte: (2 M CuCl, 8 M HCl), Separator: (Daramic-CL), Flow rate: (220 mL min^{-1}), Temperature (60 °C) (Lloyd et al., 2015).
[b]Electrodes: (FR-10 carbon felt; positive, CM 119-28; negative), Electrolyte: (2 M CuCl, 6 M HCl), Separator: (FAP-330), Flow rate: (30 mL min^{-1}), Temperature: (60 °C). (A) 25 cm^2 redox flow cell. (B) miniaturized redox flow cell.

average current efficiency of 97%. Simultaneously, the reduction in the self-discharge rate allowed for operation of the miniaturized CuRFB for over 210 h without electrolyte regeneration or replacement. With the capacity decreasing to 32% over this 210-hour period, resulting in a meaningful increase in the operational time of the CuRFB before electrolyte regeneration is required.

While the performance of the CuRFB has been improved over previous iterations, further work is still required to ready the technology for up-scaling and increasing the operational lifetime. This work can possibly entail the manufacturing and testing of low-cost separators, flow field optimization, electrolyte regeneration, and management systems for the operation of the CuRFB. With further research, the CuRFB could become cost-competitive with other solutions such as the VRFB and ICRFB.

CRediT authorship contribution statement

Wouter Dirk Badenhorst: Conceptualization, Methodology, Software, Validation, Formal analysis, Investigation, Data curation, Writing – original draft, Writing – review & editing, Visualization. **Kuldeep:** Methodology, Investigation, Writing – review & editing, Visualization. **Laura Sanz:** Conceptualization, Methodology, Writing – review & editing, Funding acquisition. **Catia Arbizzani:** Conceptualization, Methodology, Writing – review & editing. **Lasse Murtomäki:** Conceptualization, Methodology, Writing – review & editing, Funding acquisition, Supervision, project administration.

Declaration of competing interest

The authors declare that they have no known competing financial interests or personal relationships that could have appeared to influence the work reported in this paper.

Acknowledgments

We would like to thank VisBlue A/S for their assistance in designing the redox flow cell, Jani Kalasniemi from the Aalto Design Factory, and Seppo Jääskeläinen from the Department workshop assistance for the manufacturing. In addition to this, we would like to thank Seyedabolfazl Mousavi for his assistance in preparing and analyzing the samples for scanning electron microscopy analysis.

Funding

The research was performed within the CuBER project funded by the EU Horizon 2020 Program (H2020/2014-2020), grant #875605.

Appendix A. Supplementary data

Supplementary material related to this article can be found online at https://doi.org/10.1016/j.egyr.2022.06.075.

References

AlShafi, M., Bicer, Y., 2021. Life cycle assessment of compressed air, vanadium redox flow battery, and molten salt systems for renewable energy storage. Energy Rep. 7, 7090–7105. http://dx.doi.org/10.1016/j.egyr.2021.09.161.
Alva, G., Lin, Y., Fang, G., 2018. An overview of thermal energy storage systems. Energy 144, 341–378. http://dx.doi.org/10.1016/j.energy.2017.12.037.
Bard, A.J., Faulkner, L.R., 2001. Fundamentals and applications. Electrochem. Methods 2, 580–632.
Beukes, N.T., Badenhorst, J., 2009. Copper electrowinning: Theoretical and practical design. J. South. African Inst. Min. Metall. 109, 343–356.
Castillo, A., Gayme, D.F., 2014. Grid-scale energy storage applications in renewable energy integration: A survey. Energy Convers. Manag. 87, 885–894. http://dx.doi.org/10.1016/j.enconman.2014.07.063.
Cho, H., Krieg, H.M., Kerres, J.A., 2019. Performances of anion-exchange blend membranes on vanadium redox flow batteries. Membranes (Basel) 9, 31.
Faggiano, L., Lacarbonara, G., Badenhorst, W.D., Murtomäki, L., Sanz, L., Arbizzani, C., 2022. Short thermal treatment of carbon felts for copper-based redox flow batteries. J. Power Sources 520, http://dx.doi.org/10.1016/j.jpowsour.2021.230846.
Fraser, E.J., Wills, R.G.A., Cruden, A.J., 2020. The use of gold impregnated carbon-polymer electrodes with the soluble lead flow battery. Energy Rep. 6, 19–24. http://dx.doi.org/10.1016/j.egyr.2020.02.023.
Gouveia, J.R., Silva, E., Mata, T.M., Mendes, A., Caetano, N.S., Martins, A.A., 2020. Life cycle assessment of a renewable energy generation system with a vanadium redox flow battery in a NZEB household. Energy Rep. 6, 87–94. http://dx.doi.org/10.1016/j.egyr.2019.08.024.
Kologo, S., Eyraud, M., Bonou, L., Vacandio, F., Massiani, Y., 2007. Voltametry and EQCM study of copper oxidation in acidic solution in presence of chloride ions. Electrochim. Acta 52, 3105–3113. http://dx.doi.org/10.1016/j.electacta.2006.09.052.
Lacarbonara, G., Faggiano, L., Porcu, S., Ricci, P.C., Rapino, S., Casey, D.P., Rohan, J.F., Arbizzani, C., 2021. Copper chloro-complexes concentrated solutions: An electrochemical study. Batteries 7, 83. http://dx.doi.org/10.3390/batteries7040083.
Leung, P., Shah, A.A., Sanz, L., Flox, C., Morante, J.R., Xu, Q., Mohamed, M.R., Ponce de León, C., Walsh, F.C., 2017. Recent developments in organic redox flow batteries: A critical review. J. Power Sources 360, 243–283. http://dx.doi.org/10.1016/j.jpowsour.2017.05.057.
Lloyd, D., Magdalena, E., Sanz, L., Murtomäki, L., Kontturi, K., 2015. Preparation of a cost-effective, scalable and energy efficient all-copper redox flow battery. J. Power Sources 292, 87–94. http://dx.doi.org/10.1016/j.jpowsour.2015.04.176.
Martinez-Lombardia, E., Gonzalez-Garcia, Y., Lapeire, L., De Graeve, I., Verbeken, K., Kestens, L., Mol, J.M.C., Terryn, H., 2014. Scanning electrochemical microscopy to study the effect of crystallographic orientation on the electrochemical activity of pure copper. Electrochim. Acta 116, 89–96. http://dx.doi.org/10.1016/j.electacta.2013.11.048.
Nieminen, E., Murtomäki, L., 2021. Kinetics of Cu2+ reduction and nanoparticle nucleation at micro-scale 1, 2-dichlorobenzene-water interface studied by cyclic voltammetry and square-wave voltammetry. Electroanalysis http://dx.doi.org/10.1002/elan.202100172.

Ruan, W., Mao, J., Yang, S., Shi, C., Jia, G., Chen, Q., 2020. Designing Cr complexes for a neutral Fe-Cr redox flow battery. Chem. Commun. 56, 3171–3174. http://dx.doi.org/10.1039/c9cc09704j.

Rufer, A., 2020. Design and control of a KE (kinetic energy) - compensated gravitational energy storage system. In: 2020 22nd Eur. Conf. Power Electron. Appl. EPE 2020 ECCE Eur. http://dx.doi.org/10.23919/EPE20ECCEEurope43536.2020.9215714.

Sánchez-Díez, E., Ventosa, E., Guarnieri, M., Trovò, A., Flox, C., Marcilla, R., Soavi, F., Mazur, P., Aranzabe, E., Ferret, R., 2021. Redox flow batteries: Status and perspective towards sustainable stationary energy storage. J. Power Sources 481, http://dx.doi.org/10.1016/j.jpowsour.2020.228804.

Sanz, L., Lloyd, D., Magdalena, E., Palma, J., Kontturi, K., 2014. Description and performance of a novel aqueous all-copper redox flow battery. J. Power Sources 268, 121–128. http://dx.doi.org/10.1016/j.jpowsour.2014.06.008.

Sanz, L., Palma, J., García-Quismondo, E., Anderson, M., 2013. The effect of chloride ion complexation on reversibility and redox potential of the Cu(II)/Cu(I) couple for use in redox flow batteries. J. Power Sources 224, 278–284. http://dx.doi.org/10.1016/j.jpowsour.2012.10.005.

Starosvetsky, D., Khaselev, O., Auinat, M., Ein-Eli, Y., 2006. Initiation of copper dissolution in sodium chloride electrolytes. Electrochim. Acta 51, 5660–5668. http://dx.doi.org/10.1016/j.electacta.2006.01.058.

Sukkar, T., Skyllas-Kazacos, M., 2004. Membrane stability studies for vanadium redox cell applications. J. Appl. Electrochem. 34, 137–145. http://dx.doi.org/10.1023/B:JACH.0000009931.83368.dc.

Wei, X., Li, L., Luo, Q., Nie, Z., Wang, W., Li, B., Xia, G.G., Miller, E., Chambers, J., Yang, Z., 2012. Microporous separators for Fe/V redox flow batteries. J. Power Sources 218, 39–45. http://dx.doi.org/10.1016/j.jpowsour.2012.06.073.

Wu, M.C., Zhao, T.S., Jiang, H.R., Zeng, Y.K., Ren, Y.X., 2017. High-performance zinc bromine flow battery via improved design of electrolyte and electrode. J. Power Sources 355, 62–68. http://dx.doi.org/10.1016/j.jpowsour.2017.04.058.

Zeng, Y.K., Zhou, X.L., An, L., Wei, L., Zhao, T.S., 2016. A high-performance flow-field structured iron–chromium redox flow battery. J. Power Sources 324, 738–744. http://dx.doi.org/10.1016/j.jpowsour.2016.05.138.

Zhao, H., Chang, J., Boika, A., Bard, A.J., 2013. Electrochemistry of high concentration copper chloride complexes. Anal. Chem. 85, 7696–7703. http://dx.doi.org/10.1021/ac4016769.